BULLETIN OF THE EARTHQUAKE
RESEARCH INSTITUTE
UNIVERSITY OF TOKYO
Vol. 65 (1990) pp. 105-133

Report on DELP 1986 Cruises in the Northwestern Pacific Part III: Seismic Structure Revealed by Explosion Experiments

Shozaburo NAGUMO[1], Atsuki KUBO[2], Toru OUCHI[2], Hiroshi KATAO[3] and Sadayuki KORESAWA[3]

1) Hawaii Institute of Geophysics, University of Hawaii
2) Department of Earth Science, Kobe University
3) Earthquake Research Institute, University of Tokyo

(Received September 27, 1989)

Abstract

Several interesting features of the crust to upper mantle structure beneath the Northwest Pacific Basin were revealed by a seismic explosion experiment conducted during the DELP cruises in 1986. A large lateral heterogeneity was found both in the configuration of the crust/mantle structure and in the sub-Moho lithosphere. The data from the long range explosion experiment along the WSW-ENE survey line do not support the speculation of large scale anisotropy in this region. The lateral heterogeneities in the crust/mantle structure are indicated by variations of the velocity gradients within oceanic layer 3 and in the velocity transitions from layer 3 to the upper mantle. Wide-angle reflections from inside the sub-Moho lithosphere are clearly recorded with a good signal to noise ratio by small explosions of only 20 kg at distances as far as 450 km. However, the appearance of these phases differs from place to place. In some places, they are not observed. Lateral heterogeneity of this reflective layer seems to be related to such tectonic features as the fracture zone as well as Nakwe deepsea channel.

1. Introduction

We will outline features of the crust and upper-mantle structure revealed by the seismic explosion experiment coducted during the DELP 1986 cruise in the Northwest Pacific Basin. Topographic features and

configuration of seismic experiment are presented in Fig. 1. Since the outline of the seismic experiment is described in Part 1 of this cruise report, we will describe results of structure analyses obtained from the EOBS (Earthquake Research Institute Ocean Bottom Seismometer with hydrophone) stations 1 through 6 shown in Fig. 1. This report consists of three sections, Section 2 for the explosion experiment of small dynamite charges, Section 3 for the large explosion experiment of large shots and Section 4 for wide-angle reflections from the sub-Moho lithosphere.

2. Crust to mantle structure

Record sections are presented in Figs. 3, 4 and 5 which are obtained at three stations EOBS1, 3 and 6 among five EOBSs deployed along the NNW-SSE survey line. The locations of these stations and their associated shooting lines are shown in Fig. 2 and listed in Table 1 and 2.

The Station EOBS6 is located at the intersection of the two long range survey lines; one about 1400 km in ENE-WSW direction and the other about 700 km in NNW-SSE direction. EOBS6 is located on the flank of the NE-SW trending Hokkaido Rise (see Fig. 1), EOBS1 in the eastern

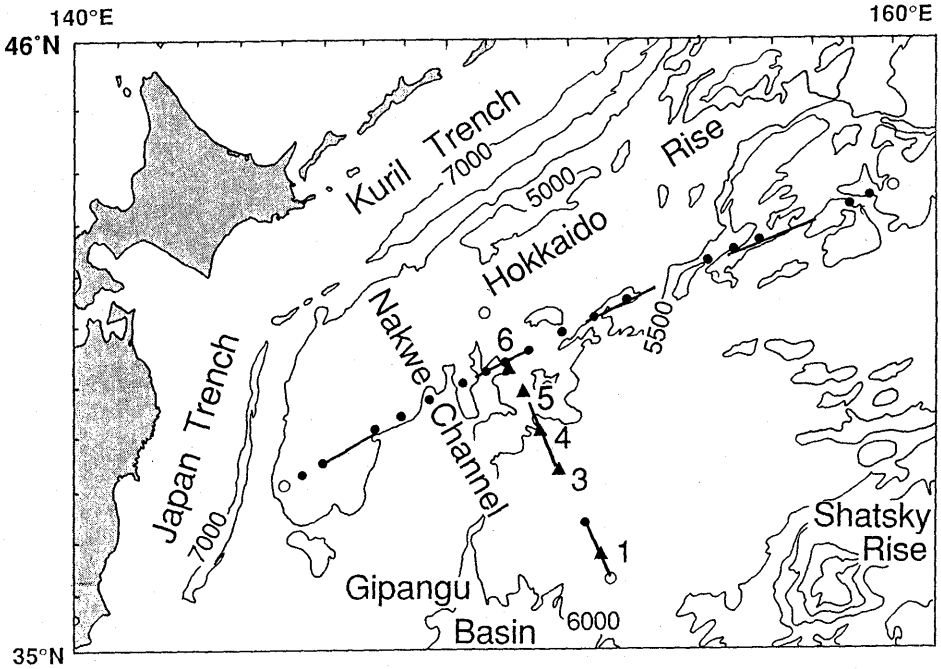

Fig. 1. Index map of seismic experiment of the cruise. Symbols about seismic experiment are explained in Fig. 2.

margin of the Gipangu Basin, and EOBSs near the SE-facing rim of the Hokkaido Rise. The NNW-SSE direction survey line is roughly parallel to, and about 100 km east of the deep sea channel called Nakwe channel (MAMMERICKX, 1980; bathymetric map) (MAMMERICKX and SMITH, 1985). This channel runs southward from the Hokkaido Rise south to the Gipangu Basin. This NNW-SSE line was positioned to avoid fracture zones.

The bathymetric profiles along the shooting lines are shown in Fig. 6, which will be used for identifying the phase alignment on the record sections in which water depth corrections are not applied. In the shooting line F for EOBS1, the effect of a seamount about 1 km high near the NNW end of the line should be taken into consideration for interpreting the apparent velocities. Also in the shooting line C for EOBS6, the effect of a small seamount about seven hundred meters high in the WSW side of the station should be carefully treated.

Appearances of refraction from layer 3 or wide angle reflection from the layer 3/mantle boundary (hereafter we refer to these two simply as

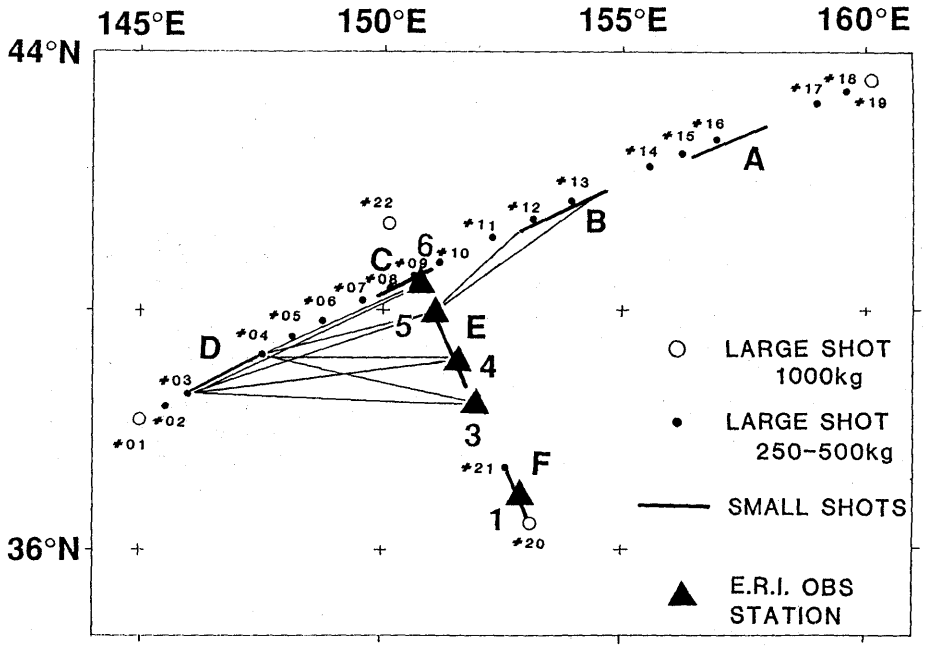

Fig. 2. Configurations of seismic experiment in this cruise. Solid triangles are EOBSs (1-6). Solid lines mean small explosive shots (A-F). The large explosive shots in the WSW-ENE direction are presented by solid and open circles (shots No. 1-19). The amount of explosives: 1 ton for shots No. 1, 19, 20, and 22; 500 kg for shots No. 2 through 18, and 21. Fans enclosed by two thin lines between OBS and shot points indicate paths where wide angle reflections are observed (see details in section 4).

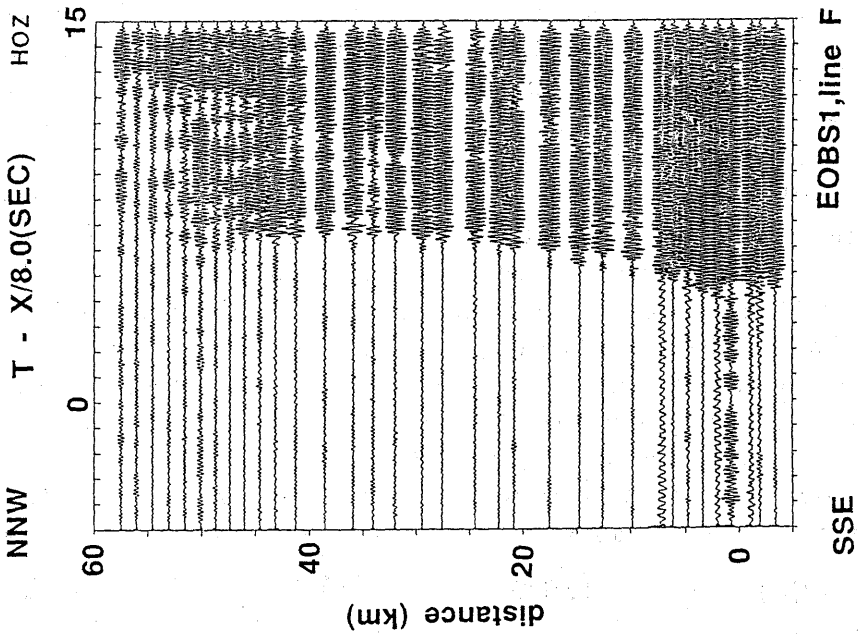

3(b) horizontal component,

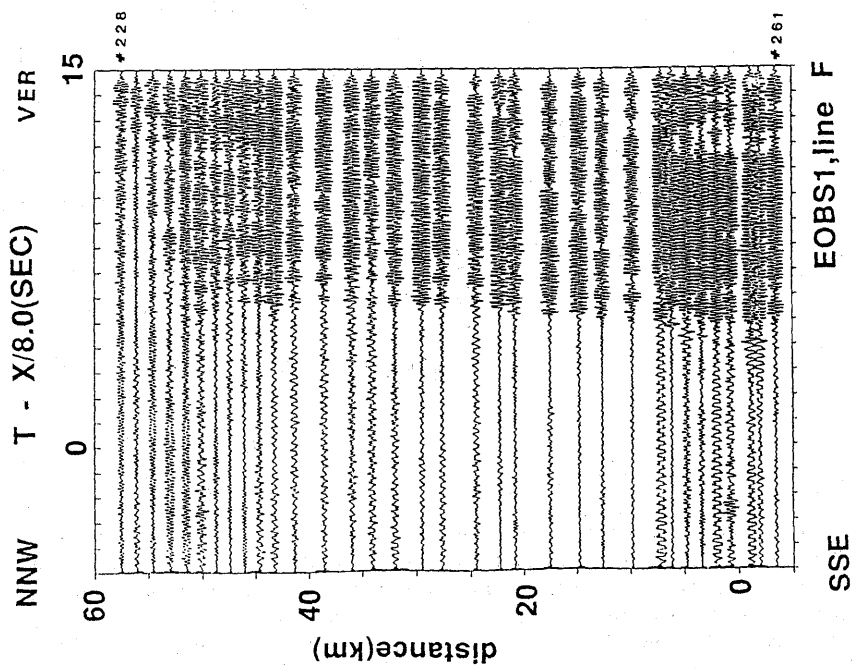

3(a) vertical component,

Fig. 3. Record sections of EOBS1 for high density shot line F. Filter : 4-20 Hz.

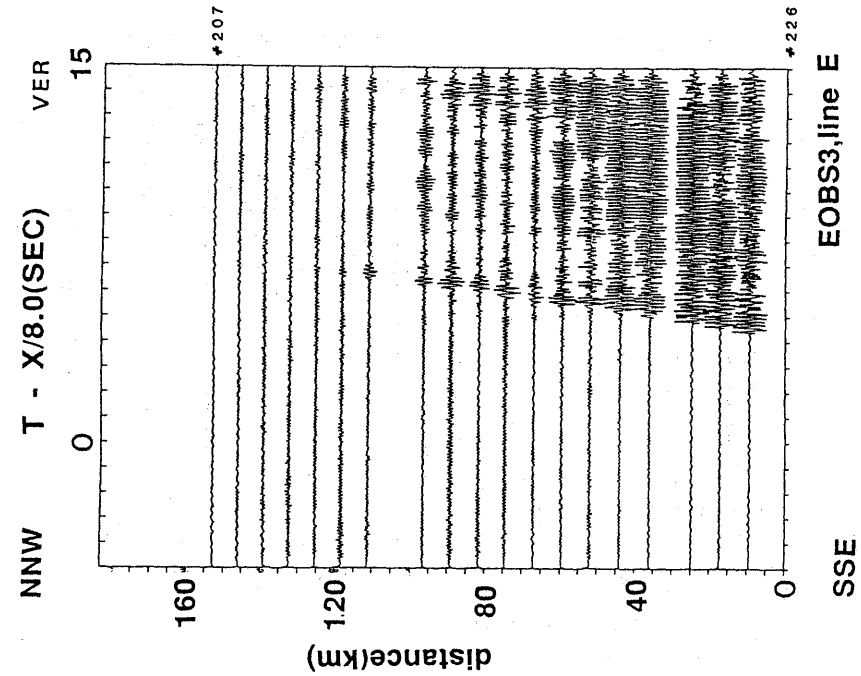

4(a) vertical component,

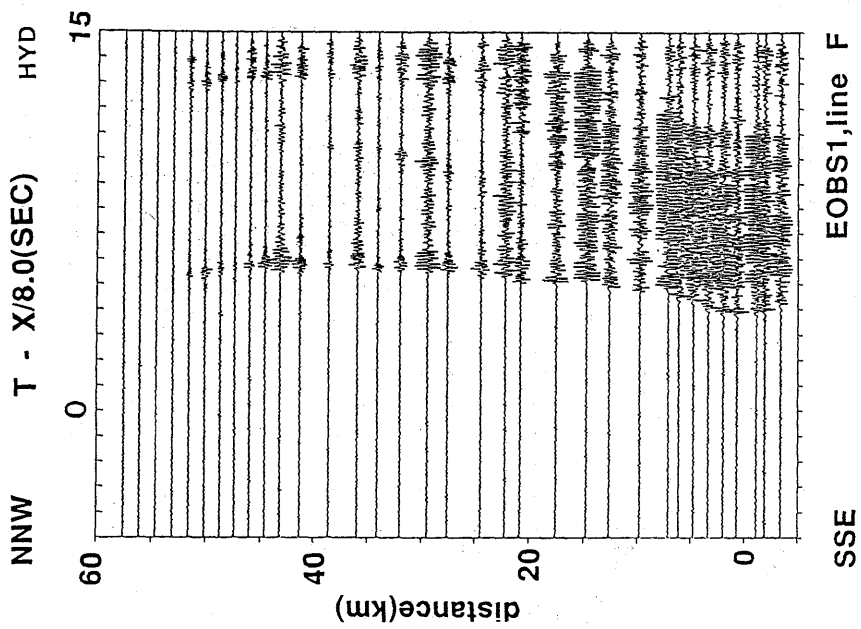

3(c) hydrophone.

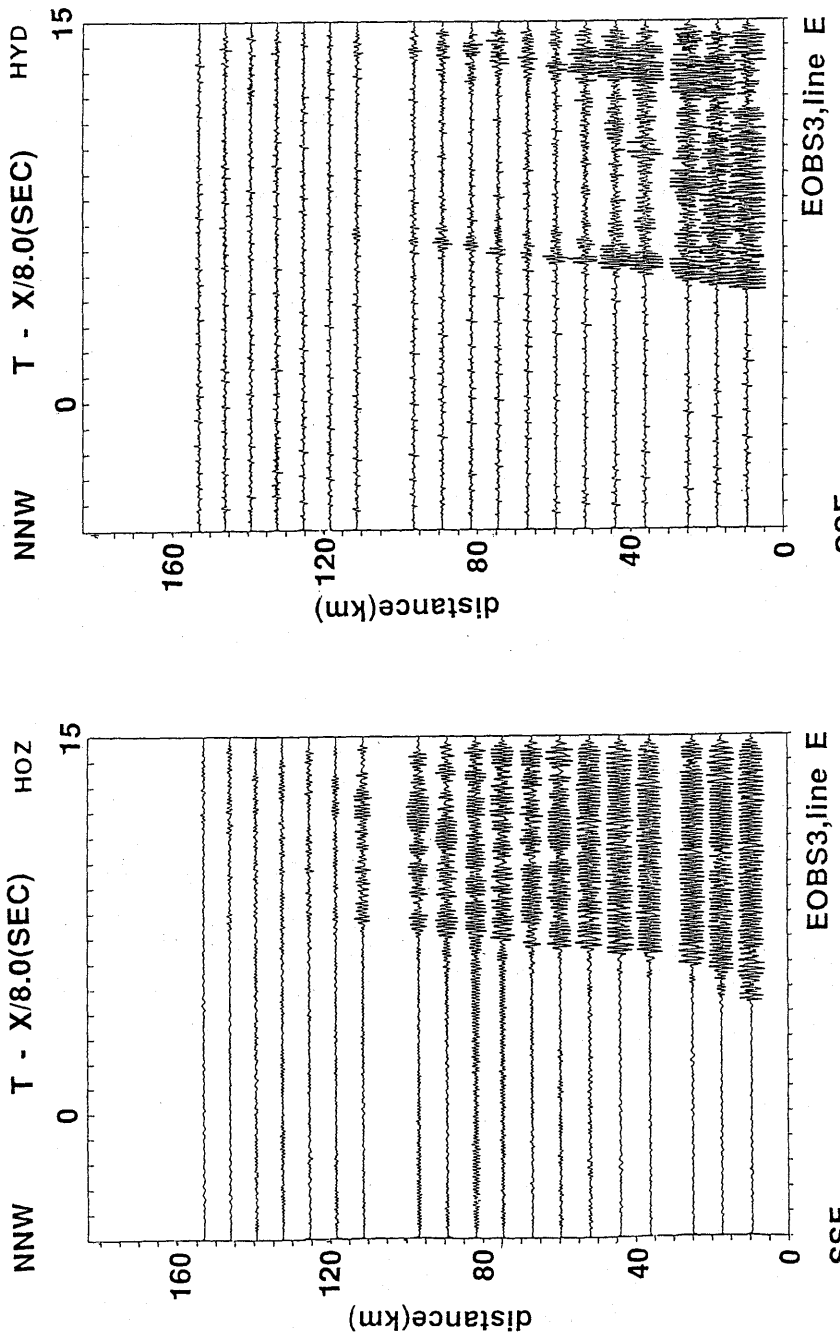

4(b) horizontal component, 4(c) hydrophone.

Fig. 4. Record sections of EOBS3 for shot line E. Filter : 4-20 Hz.

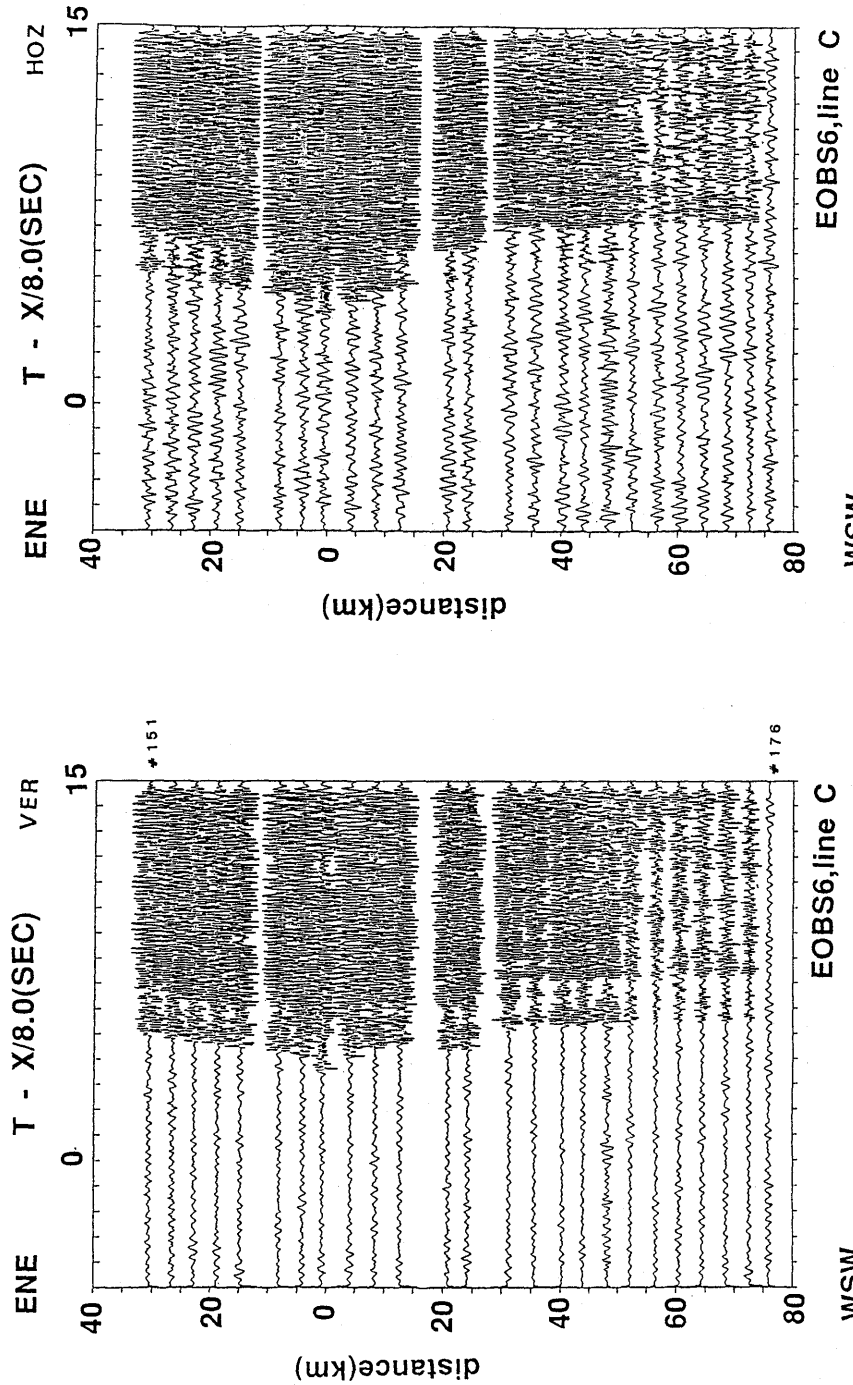

5(a) vertical component,

5(b) horizontal component,

Fig. 5. Record sections of EOBS6 for shot line C. Filter : 4-20 Hz.

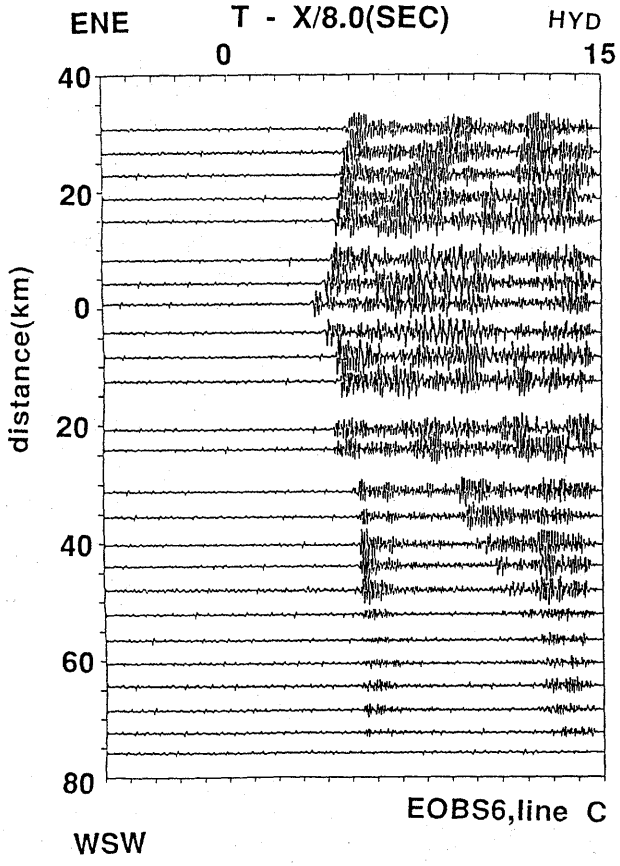

5(c) hydrophone.

Table 1. Earthquake Research Institute OBS's location data.

OBS No.	Latitude		Longitude		Water Depth
------	(deg.)	(min.)	(deg.)	(min.)	(meter)
EOBS1	36	53.56	152	52.86	5680
EOBS3	38	39.15	151	49.77	5685
EOBS4	39	11.67	151	29.72	5472
EOBS5	40	08.28	150	54.18	5390
EOBS6	40	32.51	150	38.35	5432

Table 2. Small shot data for each line.

Shot No	Date	Shot time (h)	(m)	(s)	Latitude (deg.)	(min.)	Longitude (deg.)	(min.)	W.Dep. (m)	Azim. (deg)	Weight (kg)
						N		E			
151	7/22	06	52	04.723	40	39.38	150	57.87	5410	241	20
152	7/22	07	12	08.014	40	38.28	150	55.34	5422	243	20
153	7/22	07	32	01.081	40	37.34	150	52.96	5390	244	20
154	7/22	07	52	06.495	40	36.40	150	50.35	5302	245	20
155	7/22	08	12	03.652	40	35.48	150	47.83	5403	247	20
156	7/22	08	41	56.730	40	33.91	150	43.57	5282	248	20
157	7/22	09	02	03.339	40	33.01	150	40.95	5386	247	20
158	7/22	09	22	04.534	40	32.03	150	38.37	5442	246	20
159	7/22	09	42	05.148	40	31.11	150	35.72	5453	245	20
160	7/22	10	02	05.481	40	30.07	150	32.93	5477	246	20
161	7/22	10	22	06.411	40	29.07	150	30.33	5493	246	20
162	7/22	10	42	07.136	40	28.13	150	27.69	5215	247	20
163	7/22	11	02	04.282	40	27.15	150	25.13	4866	245	20
164	7/22	11	17	07.423	40	26.34	150	23.00	4999	246	20
165	7/22	11	52	02.462	40	24.72	150	18.47	5538	246	20
166	7/22	12	12	01.653	40	23.73	150	15.79	5439	247	20
167	7/22	12	35	02.291	40	29.52	150	12.74	5417	246	20
168	7/22	12	52	03.481	40	21.67	150	10.46	5398	246	20
169	7/22	13	12	03.204	40	20.64	150	07.82	5431	247	20
170	7/22	13	32	05.203	40	19.64	150	05.23	5378	245	20
171	7/22	13	53	06.413	40	18.57	150	02.53	5400	246	20
172	7/22	14	12	03.099	40	17.53	150	00.06	5561	247	20
173	7/22	14	32	06.090	40	16.50	149	57.62	5529	247	20
174	7/22	14	52	04.839	40	15.45	149	55.05	5513	249	20
175	7/22	15	12	07.143	40	14.48	149	52.60	5520	249	20
176	7/22	15	27	07.075	40	13.59	149	50.49	5538	249	20
177	7/22	06	52	04.723	40	39.38	150	57.87	5410	241	20
207	7/26	05	44	59.583	39	53.97	151	05.33	5420	157	20
208	7/26	06	14	59.883	39	50.78	151	07.66	5413	157	20
209	7/26	06	45	00.273	39	47.51	151	09.94	5446	160	20

210	7/26	07 15 00.173	39 44.12	151 11.80	5383	162	20
211	7/26	07 45 00.296	39 40.56	151 13.49	5327	167	20
212	7/26	08 15 00.205	39 37.26	151 15.85	5272	162	20
213	7/26	08 45 00.336	39 33.70	151 17.97	5304	159	20
214	7/26	09 15 00.450	39 30.10	151 20.06	5409	161	20
215	7/26	09 45 00.067	39 26.57	151 22.33	5123	157	20
216	7/26	10 15 00.275	39 23.01	151 24.64	5401	158	20
217	7/26	10 45 00.677	39 19.39	151 27.05	5519	159	20
218	7/26	11 15 00.640	39 15.92	151 29.16	5474	168	20
219	7/26	11 45 00.502	39 12.13	151 31.12	5464	167	20
220	7/26	12 14 59.901	39 08.41	151 32.95	5591	166	20
221	7/26	12 45 00.564	39 04.45	151 34.70	5741	167	20
222	7/26	13 15 00.581	39 00.46	151 36.77	5632	166	20
223	7/26	13 45 00.521	38 56.50	151 38.76	5654	159	20
224	7/26	14 43 00.424	38 50.98	151 42.04	5734	157	20
225	7/26	15 13 00.582	38 47.36	151 44.59	5674	158	20
226	7/26	15 43 00.343	38 43.61	151 47.12	5617	157	20
227	7/27	07 48 18.377	37 22.63	152 36.65	5833	152	5
228	7/27	07 54 17.755	37 21.90	152 37.31	5394	151	5
229	7/27	08 00 01.643	37 21.26	152 37.95	5106	152	5
230	7/27	08 05 33.642	37 20.49	152 38.30	5060	157	5
231	7/27	08 11 18.974	37 19.73	152 38.73	5013	159	5
232	7/27	08 17 41.381	37 18.92	152 39.28	4794	160	20
233	7/27	08 22 29.156	37 18.37	152 39.77	4846	158	5
234	7/27	08 28 04.562	37 17.63	152 39.93	4996	160	5
235	7/27	08 33 37.766	37 16.98	152 40.38	5153	159	5
236	7/27	08 39 11.414	37 16.24	152 40.57	5367	158	5
237	7/27	08 44 44.324	37 15.56	152 41.02	5830	159	5
238	7/27	08 49 34.134	37 15.14	152 41.25	5772	159	20
239	7/27	09 01 18.511	37 13.91	152 41.87	5787	159	20
240	7/27	09 12 21.209	37 12.61	152 42.75	5769	155	5
241	7/27	09 21 59.787	37 11.61	152 43.37	5765	155	20
242	7/27	09 34 19.794	37 10.45	152 44.16	5834	154	5
243	7/27	09 45 20.926	37 09.49	152 44.83	5804	155	5

244	7/27	09 55 00.273	37 08.52	152 45.46	5767		20
245	7/27	10 07 13.467	37 07.37	152 46.35	5760	149	5
246	7/27	10 18 18.332	37 06.06	152 48.04	5758	150	5
247	7/27	10 28 00.375	37 05.11	152 48.04	5679	150	20
248	7/27	10 40 20.793	37 04.14	152 48.65	5775	160	5
249	7/27	10 51 16.934	37 02.47	152 49.35	5795	164	5
250	7/27	11 01 00.355	37 01.31	152 49.71	5765	164	20
251	7/27	11 13 17.784	36 59.84	152 50.07	5797	164	5
252	7/27	11 24 17.353	36 58.35	152 50.51	5835	165	5
253	7/27	11 34 00.307	36 57.21	152 50.84	5778	165	20
254	7/27	11 41 48.173	36 56.42	152 51.22	5814	159	5
255	7/27	11 47 17.777	36 55.71	152 51.49	5828	160	5
256	7/27	11 52 53.082	36 55.01	152 51.85	5864	158	5
257	7/27	11 58 22.709	36 54.29	152 52.15	5822	158	5
258	7/27	12 03 49.026	36 53.59	152 52.49	5713	157	5
259	7/27	12 09 00.321	36 53.11	152 52.75	5599	157	20
260	7/27	12 17 18.591	36 52.37	152 53.17	5724	156	5
261	7/27	12 22 44.899	36 51.60	152 53.40	5052	154	5
262	7/27	12 28 18.862	36 51.00	152 54.01	5764	154	5
263	7/27	12 33 52.395	36 50.30	152 54.50	5776	154	5
264	7/27	12 39 20.131	36 49.60	152 54.80	5810	154	5
265	7/27	12 45 32.781	36 48.80	152 55.25	5787	154	20
266	7/27	12 56 20.892	36 47.43	152 55.92	5811	155	5
267	7/27	13 07 22.001	36 46.12	152 56.78	5816	154	5
268	7/27	13 19 02.022	36 44.66	152 57.57	5814	152	5
269	7/27	13 29 18.103	36 43.43	152 58.33	5806	153	5
270	7/27	13 40 28.567	36 42.07	152 59.25	5839	153	5
271	7/27	13 51 59.811	36 40.67	153 00.10	5841	152	20
272	7/27	14 02 21.622	36 39.45	153 01.91	5791	152	5
273	7/27	14 13 13.698	36 38.08	153 01.67	5824	152	5
274	7/27	14 25 03.592	36 36.71	153 02.61	5809	152	20
275	7/27	14 29 48.280	36 36.11	153 02.86	5797	152	5
276	7/27	14 35 19.421	36 35.53	153 03.44	5796	151	5
277	7/27	14 40 49.394	36 34.89	153 03.88	5788	152	5

278	7/27	14 46 17.544	36 34.25	153 04.30	5773	151	5
279	7/27	14 51 53.392	36 33.57	153 04.76	5748	151	5
280	7/27	14 58 05.290	36 32.84	153 05.26	5747	151	20
281	7/27	15 02 47.109	36 32.28	153 05.68	5712	152	5
282	7/27	15 08 22.326	36 31.57	153 06.01	5725	153	5
283	7/27	15 13 49.611	36 30.95	153 06.56	5749	152	5
284	7/27	15 19 22.086	96 30.23	153 06.97	5755	151	5
285	7/27	15 24 47.402	36 29.63	153 07.39	5732	152	5

W. Dep.: Water depth
Azim.: Heading azimuth of the vessel.

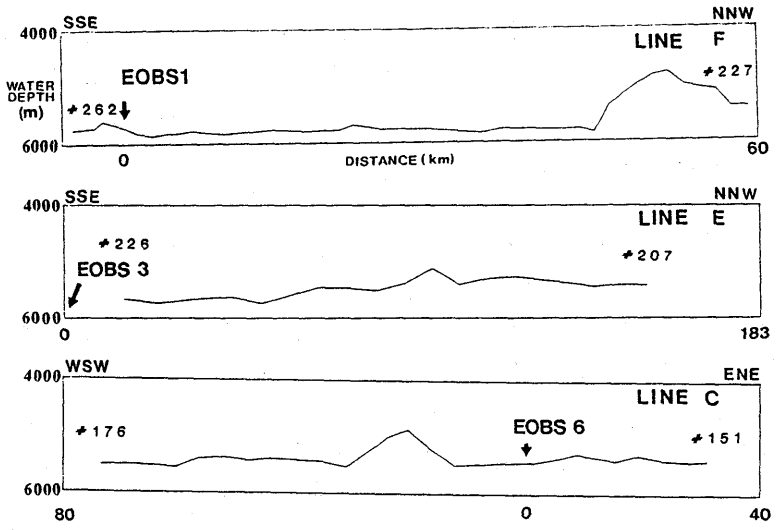

Fig. 6. Bathymetry along each small explosive shot line.

P_3), P_n, and P_mP on the record sections are quite different from station to station. On the record section of EOBS3 shown in Fig. 4, this P_3 is very clear with large amplitude up to the distance of about 120 km (Fig. 4), while the amplitude of P_n is very small. On the record section of EOBS1 (Fig. 3), we do not see such a strong line-up of P_3. Instead, the P_3 phases bend into the P_n phases smoothly, forming a simple branch of the first arrival phases. On the record section of EOBS6 (Fig. 5), we see strong and less attenuated P_n up to a distance of about 70 km.

We think that such variety in the appearance of P_3 and P_n may be an indication of lateral heterogeneity in the crust/mantle structure in this

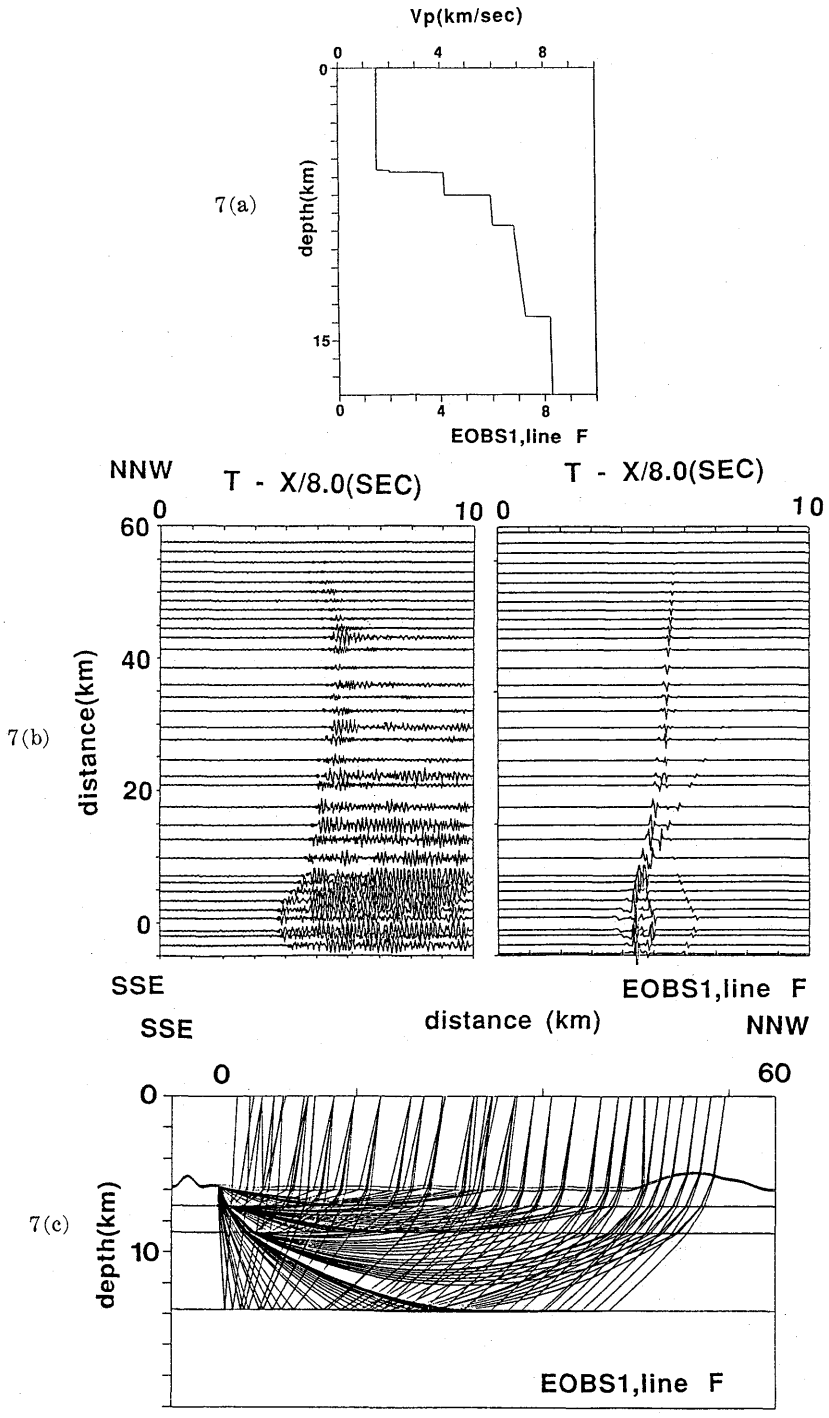

Fig. 7. (a) P velocity model for EOBS1, Line F. (b) Travel times (solid circles) computed with ray tracing and WKBJ synthetic seismogram. (c) Ray path diagram.

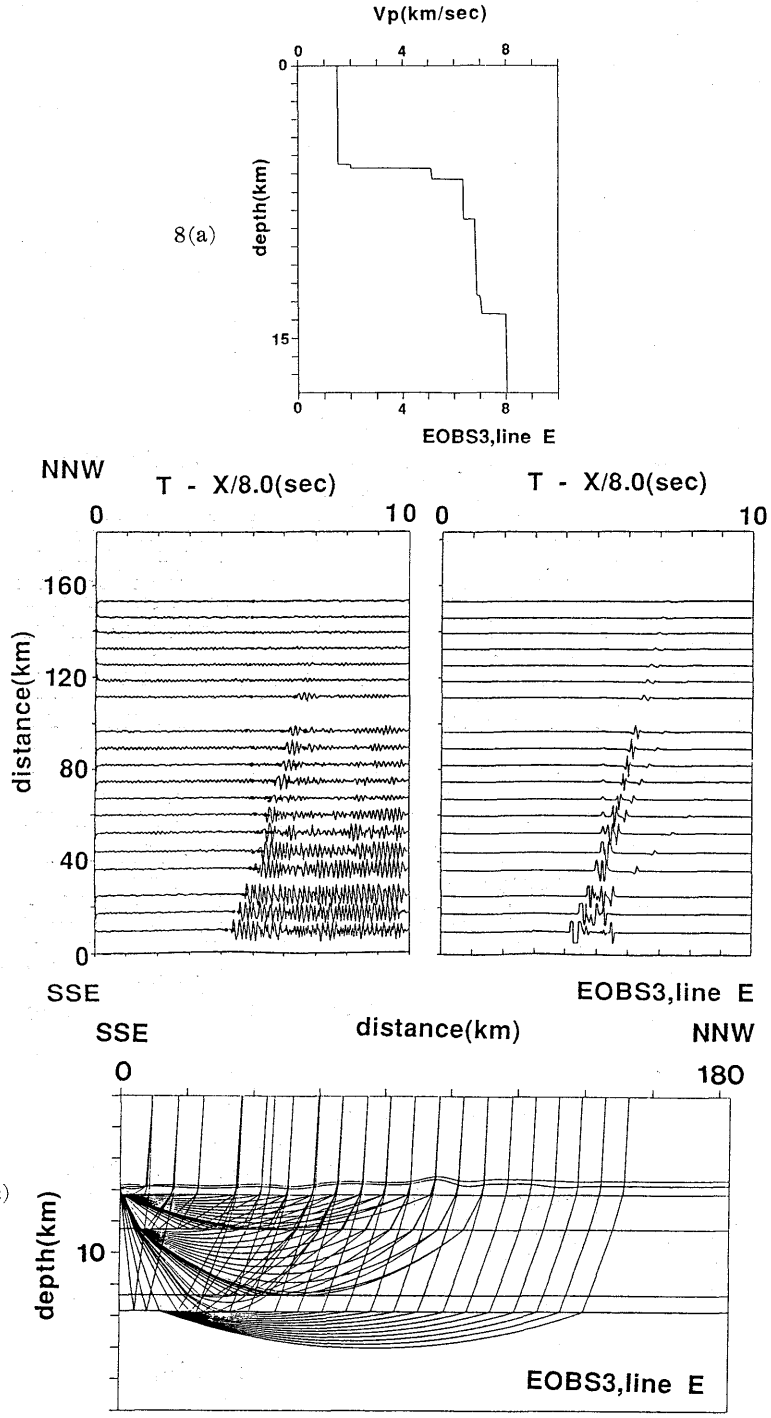

Fig. 8. (a) P velocity model for EOBS3, line E. (b) Travel times (solid circles) computed with ray tracing and WKBJ synthetic seismogram. (c) Ray path diagram.

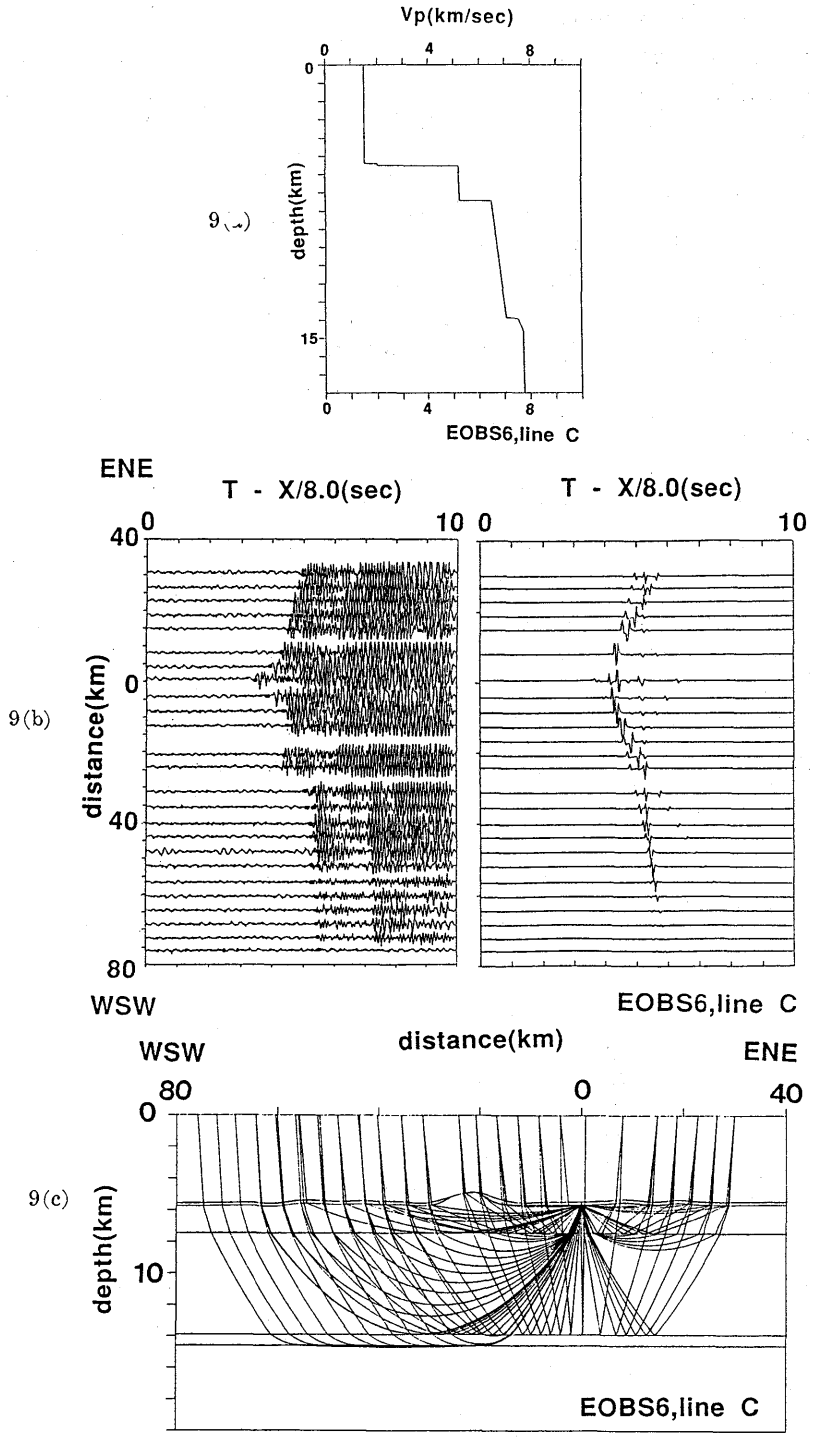

Fig. 9. (a) P velocity model for EOBS6, line C. (b) Travel times (solid circles) computed with ray tracing and WKBJ synthetic seismogram. (c) Ray path diagram.

region. Further detailed study will reveal differences of the velocity profiles among these stations. Preliminary models using ray-tracing and WKBJ synthetic seismograms are shown in Figs. 7, 8, and 9. The strong P_3 with very poor P_n seen at station EOBS3 are caused mainly by a "step" type velocity structure, which is similar to a classical layered structure (Fig. 8). Such an appearance of strong P_3 to a long distance, say about 120 km, is not due to diving P_3 refraction, but due to P_mP or wide-angle reflection from the Moho. The small amplitude of P_n is an associated consequence; they are mostly head waves along the Moho.

On the other hand, a simple bending from P_3 to P_mP on the record section of EOBS1 seem to be caused by a large velocity gradient within the layer 3 (Fig. 7). The amount of velocity step at the Moho boundary is left for further study. The large amplitudes of both P_mP and P_n without P_3 phases on the record section of EOBS6 seem to be caused by a specific structure at the transition from layer 3 to the Moho. A kind of "shoulder" type velocity profile (Fig. 9) may cause such a concentration of diving rays beyond the cross-over distance, resulting in large amplitudes in a limited distance range.

In order to see a variety of crustal structure along the survey line, preliminary P-velocity profiles of stations EOBS1, 3 and 6 are compared in Fig. 10. The crustal structure in this region is considered to be

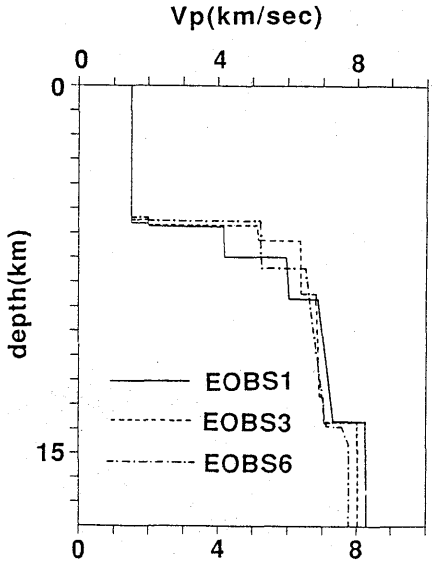

Fig. 10. Comparison of P velocity profiles among three stations.

normal oceanic having about 8 km thickness at 5.5-5.7 km beneath the seafloor. The thickness of the crust is similar to that obtained by DUENNEBIER *et al.* (1987).

Although velocity profiles are similar, some differences are apparent in the amount of velocity gradient within the layer 3 and in the detailed velocity structure of the layer 3/mantle transition. These might be important for studying the difference of petrological processes, as well as tectonic conditions which might have taken place during the generation and evolution of the oceanic crust.

3. Upper-Mantle structure

The record sections which we report here are obtained from large explosive shots (shots No. 1-19; see Table 2 of Part I of this cruis report) along the WSW-ENE direction survey line. OBS sites and shot locations are shown in Fig. 2. Station EOBS6 is located on this line, while other stations (EOBS5, 4, 3, and 1) are off-set for these shots. Topography along the survey line is shown in Fig. 11.

The length of the observation line from EOBS6 is about 550 km to the west, and about 850 km to the east. The record section provides data for WSW-ENE azimuth, almost parallel to the paleo-magnetic lineations. Such long range data are important for studying large scale 'anisotropy' in the upper mantle. The record sections are shown in Figs. 12 through 16.

The amounts of explosives are 1 ton (dispersed into 4 pieces, 250 kg each) at both ends (shots No. 1 and 19) of the survey line, and 500 kg (4 pieces, 125 kg each) at other shot points (from shot No. 2 to 18; see Table 2 of Part I of this cruise report). The shot depth was kept at 100 m below the sea surface by suspension from buoys. All large explosives were fired by electricity. The shots and OBS data are presented in Part I of this cruise report.

3.1. P_n from the Moho

On the record section of EOBS6 (Fig. 12), P_n phases are identified with an apparent velocity of about 8.0 km/s in the distance range of about 200-300 km for the western side and, 150-300 km for the eastern side of the section. The apparent early arrival at shot No. 7 (about 100 km on the west side) is caused by a bathymetric high.

The amplitude of P_n phases are sufficient to identify their coherency. Such good signal to noise ratios might be the result of the dispersed

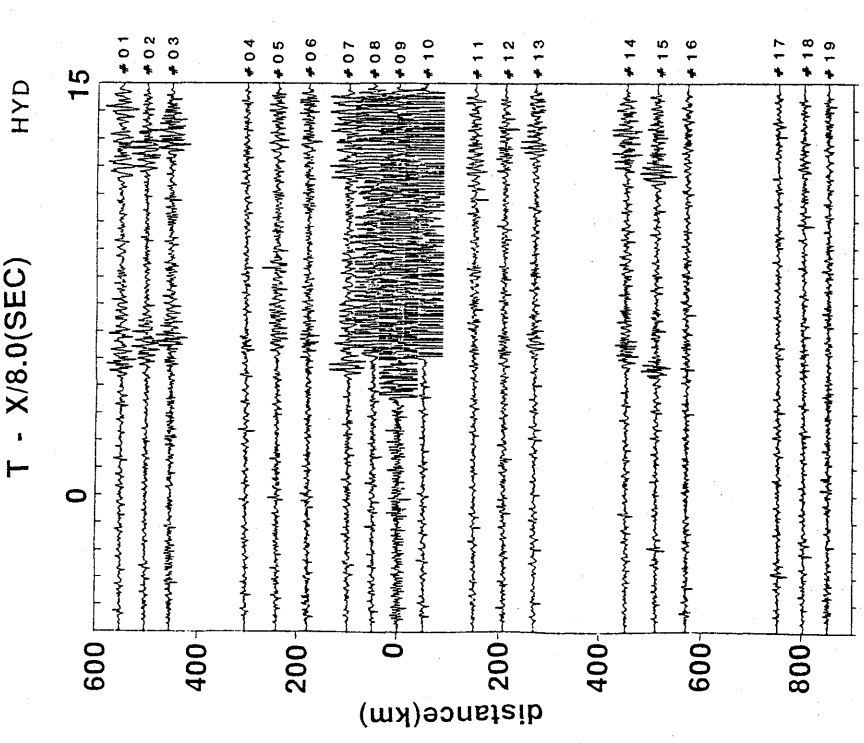

Fig. 12. Record section of EOBS6 for large explosive shots (shots No. 1 through 19), in the WSW-ENE direction (Hydrophone. Filter : 3.5-15 Hz).

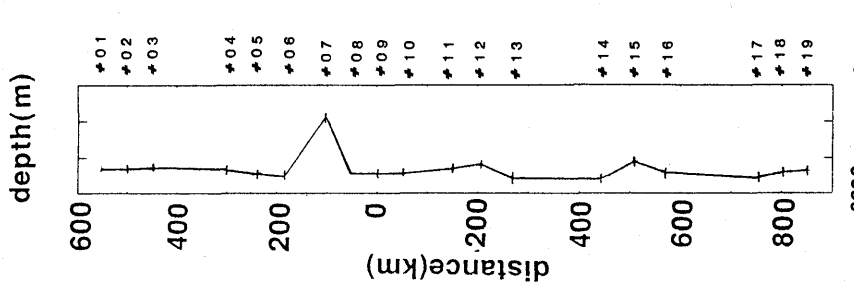

Fig. 11. Bathymetry along the WSW-ENE long range shot line.

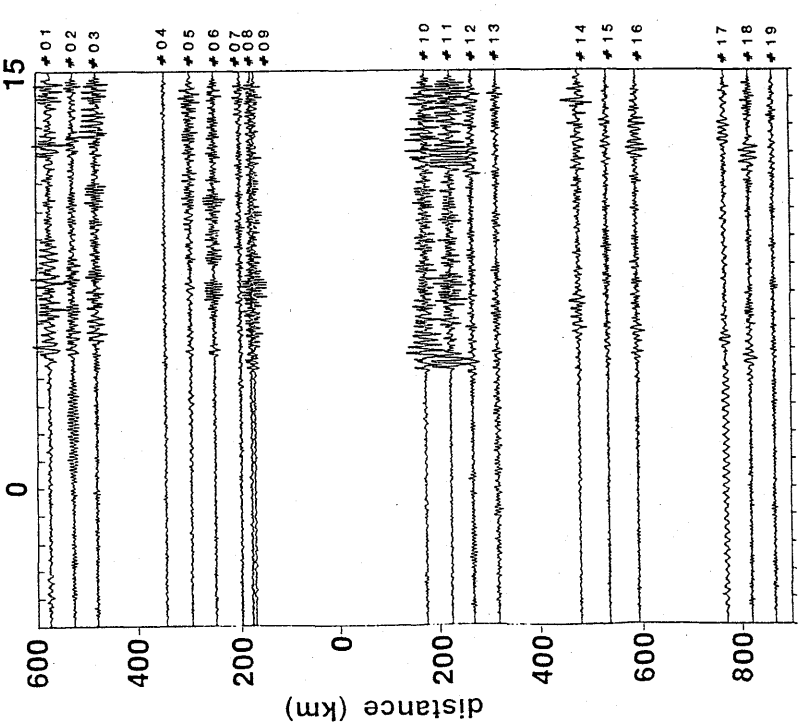

Fig. 14. Record section of EOBS4 for large explosive shots (shots No. 1 through 19), (off-set shooting, Vertical component. Filter : High Pass 4 Hz).

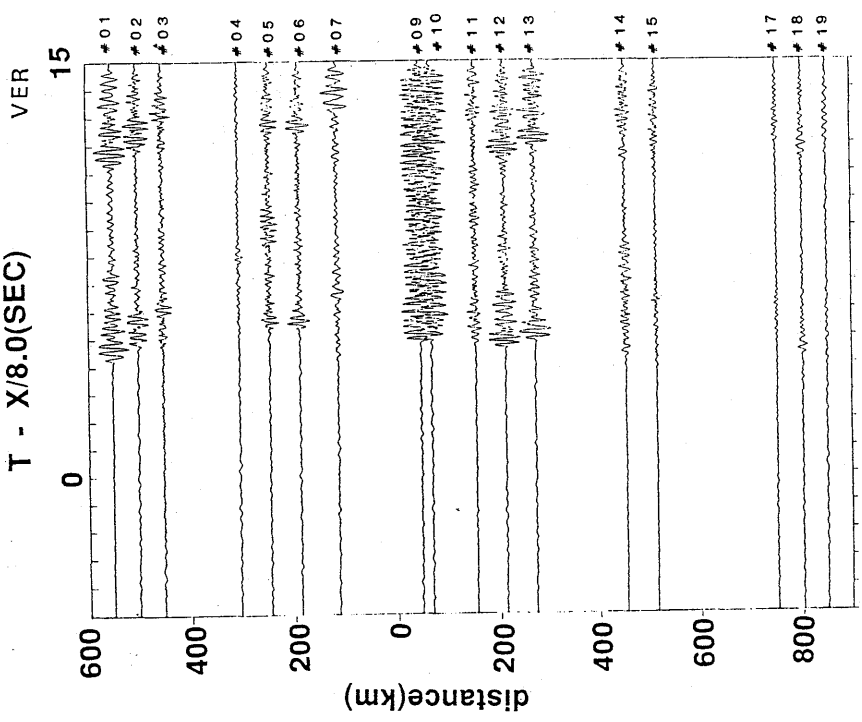

Fig. 13. Record section of EOBS5 for large explosive shots (shots No. 1 through 19), (off-set shooting, Vertical component. Filter : 4-15 Hz).

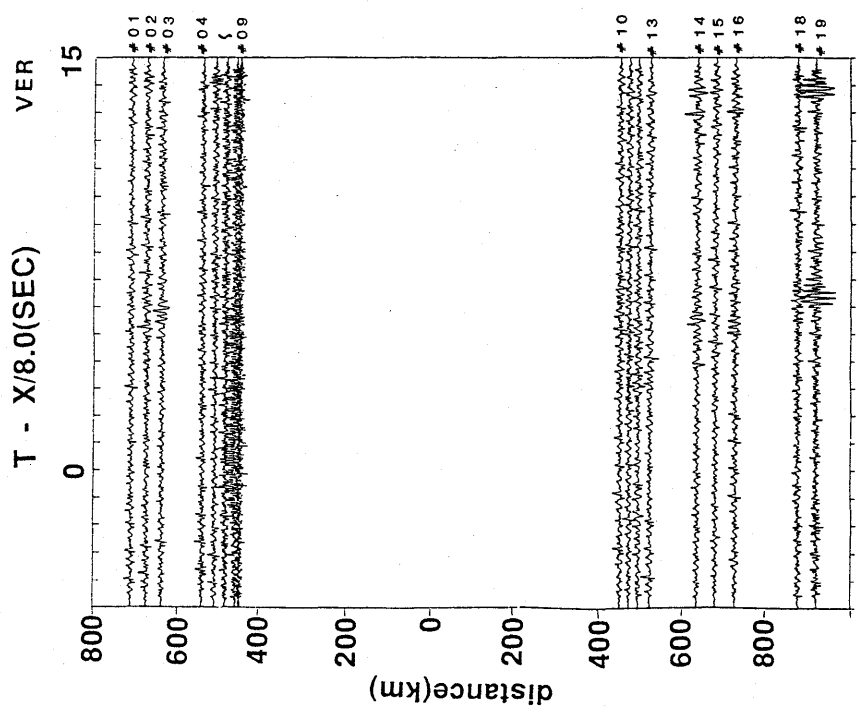

Fig. 16. Record section of EOBS1 for large explosive shots (shots No. 1-through 19), (Off-set shooting, Vertical component. Filter : High Pass 4 Hz).

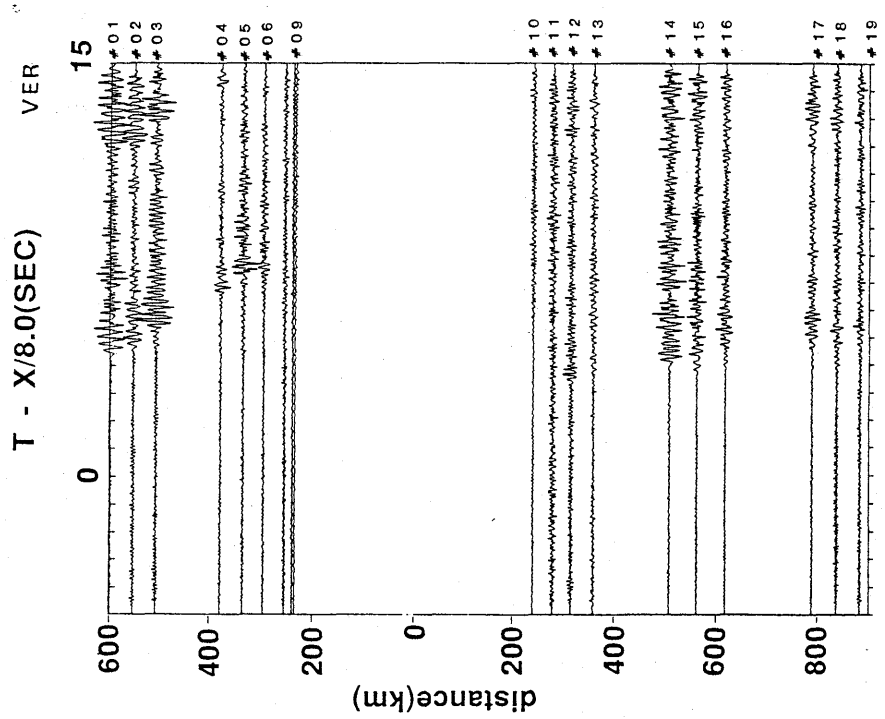

Fig. 15. Record section of EOBS3 for large explosive shots (shots No. 1-19). (Off-set shooting, Vertical component. Filter : High Pass 4 Hz).

shooting technique. The water surface reflections of these P_n phases are clearly seen about 7 second later and are of great help in identifying the real P_n phases. Larger amplitude of surface reflections than incident waves is a common feature of OBS records.

The appearance of such large amplitudes of P_n phases up to about 300 km indicates that these are diving refraction rays caused by some velocity gradient in the uppermost mantle beneath the Moho horizon.

3.2. Refraction from sub-Moho high velocity layers

Beyond about 450 km on the west side, on the traces from shot No. 1 to 3 and also beyond about 400 km on the east side from shot No. 14 to 16, we see a bend of the first arrival phases from upper-mantle refraction. The apparent velocities of these bent phases are higher than the uppermost mantle P_n velocity of 8.0 km/s, ranging from 8.2 to 8.6 km/sec. These seem to be multiple branches of travel times in this distance range. Such high apparent velocities are also identified in the sea-surface-reflection phases. The line fitting of travel-time curves for these phases is not unique because of the limited number of traces as well as the wide spacing between traces. Close inspection of these phases suggests that there are at least two high velocity layers beneath the Moho discontinuity. It is certain that there exists a stratified velocity structure in the upper-mantle along the WSW-ENE direction, although detailed structural analyses are left for future studies.

Similar large amplitudes of sub-Moho refraction are seen for shots No. 13, 14, and 15 on the east side, and appear to be caused by a similar velocity profile within the upper mantle. The disappearance of refraction from the lower lithosphere beyond about 600 km on the east side), beyond shot No. 17) may be caused by either a negative gradient in the velocity structure or large attenuation at that depth.

3.3 Large scale anisotropy

One purpose of the long range explosion experiment along the WSW-ENE direction planned in this DELP cruise was to further examine a large scale anisotropy which has been reported in the Northwest Pacific. Hitherto, for NW-SE azimuth, sub-Moho high velocity layers have been observed (ASADA and SHIMAMURA, 1976; NAGUMO *et al*, 1987). However, such high velocity layers have not been detected in several large explosion experiments (ASADA and SHIMAMURA, 1984), which had lead them to suppose the existense of large scale anisotropy in the sub-Moho lower lithosphere in this region (SHIMAMURA and ASADA, 1984). The only evi-

dence in these earlier studies for such speculation was the non-detection of high apparent velocities at long distance ranges in ENE-WSW direction.

Because of many experimental limitations, the certainty of such non-existence of the sub-Moho high volocity layers in the E-W direction has been controversial. Now that sub-Moho high apparent velocities have been detected along the WSW-ENE direction, the previous speculation of a large scale anisotropy within the upper mantle seem to have lost its basis. Instead, what we see in this experiment is large lateral heterogeneity within the upper mantle.

On the record sections for EOBS5, 4, and 3 (Figs. 13, 14, and 15), we can see similar refraction from sub-Moho high-velocity layers beyond the distance of about 400 km. The appearace of these phases are different for different stations, suggesting lateral heterogeneities. Some details of this feature will be describe in the next section.

4. Wide angle reflection from the sub-Moho lithosphere

In this section, we will briefly report on unusual upper mantle phase which will probably a wide angle reflection from inside the sub-Moho lithosphere. Such phases were observed on the record sections of EOBS4 for the small explosive shot line D (charge size 20 km each, see Fig. 2). The record section of the vertical component of EOBS4 for small explosive shot line D at distance range of about 350-450 km is shown in Fig. 17 and for the whole shot line in Fig. 18. On the record section, we can see impulsive phases having mantle apparent velocity. The amount of explosive are as small as 20 kg. The horizontal component (Fig. 19) shows large P to S conversions with a long wave train as the first arrival phases.

The apparent velocity of these phases is about 8.0 km/s, the same as the P_n velocity. In a closer distance range, from about 350 to 400 km, the line-up to these phases shows a slight bending. This bending might be a kind of diffraction effect associated with some lateral discontinuity of the reflecting horizon.

It is quite unusual that such small explosions of 20 kg are observed at the distance range of 350-450 km. Their amplitudes are nearly the same as those of P_n generated by 300-500 km explosions in the 200-300 km range. From these features, we think that these phases observed by small explosions at the distance range of about 350-450 km are not the upper-mantle refractions but a wide angle reflection from a certain interface inside the sub-Moho lithosphere. This may also be related to the mechanism of P_0 (ocean P) propagation.

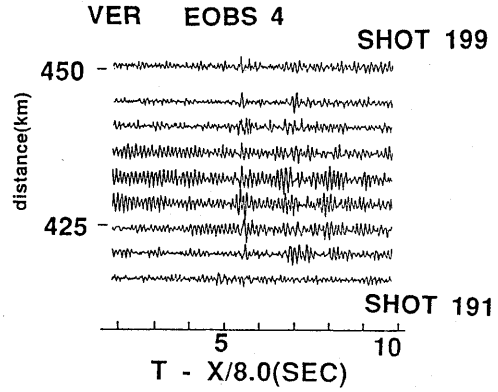

Fig. 17. Close-up of the impulsive wave forms, a part of the record section of EOBS4, for line D, vertical component.

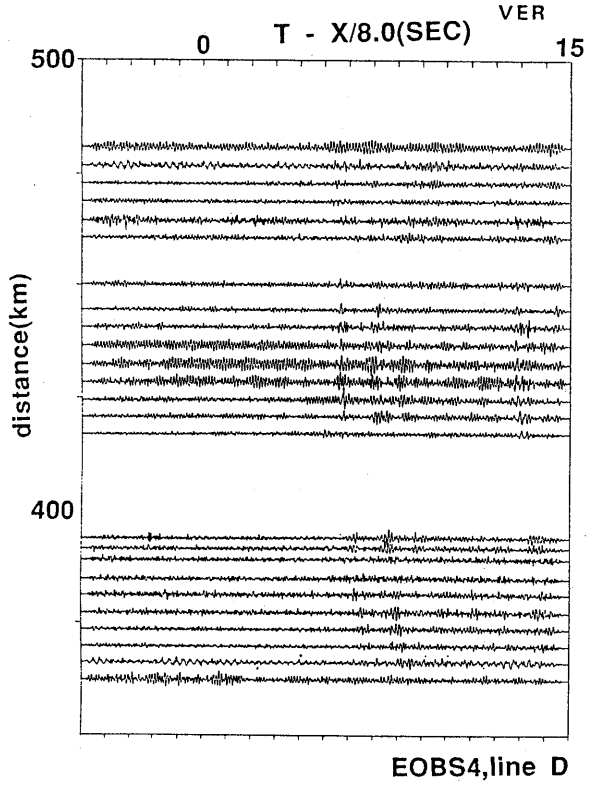

Fig. 18. Record section of EOBS4 (vertical component) for the small explosive shot line D. Filter: 4-15 Hz.

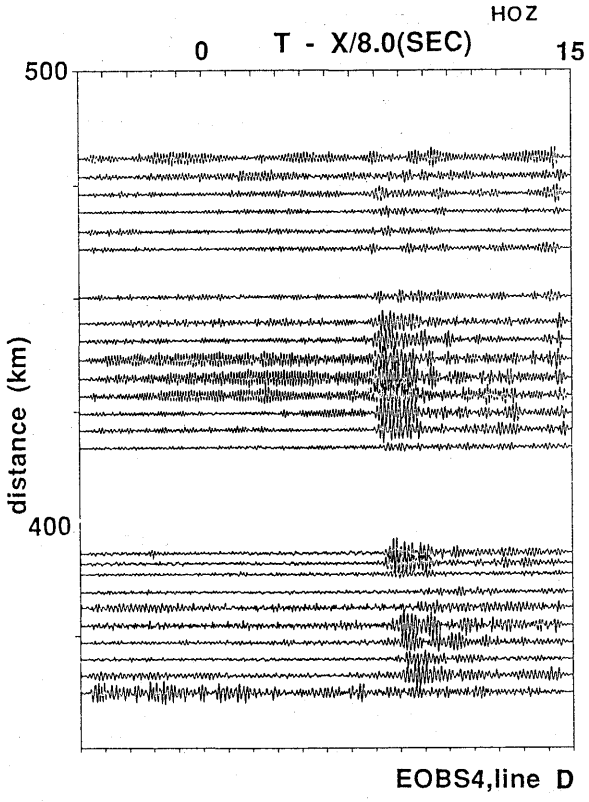

Fig. 19. Record section of EOBS4 (horizontal component) for the small explosive shot line D. Filter: 4-15 Hz.

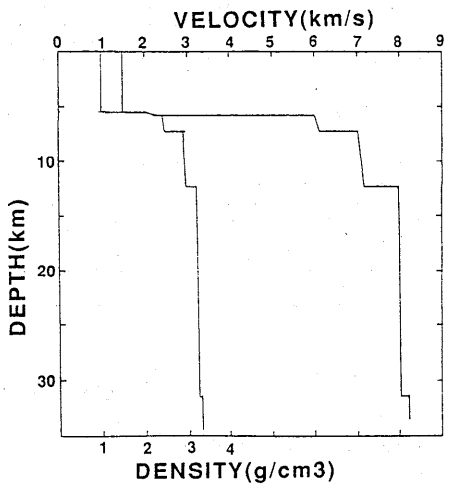

Fig. 20. Preliminary P-velocity model in the region between EOBS4 and shot line D.

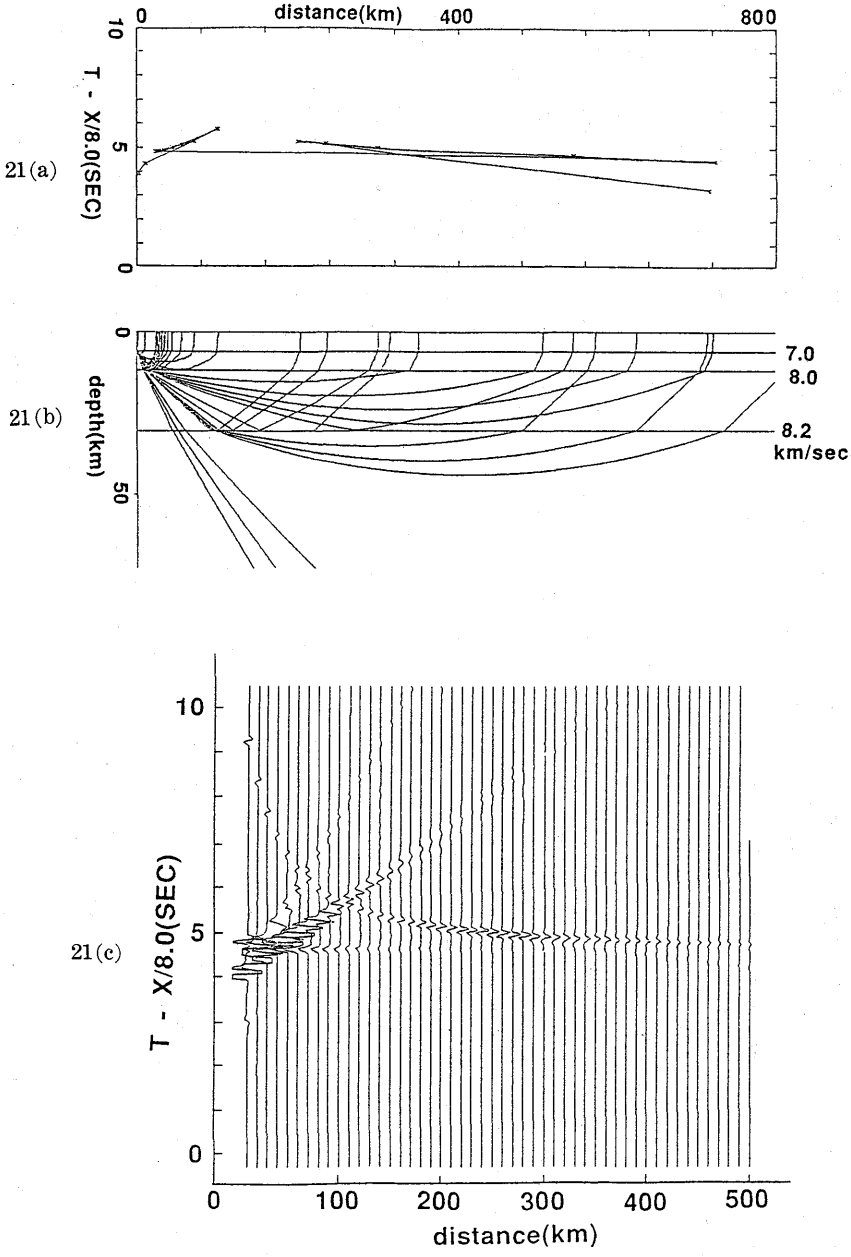

Fig. 21. (a) Travel time curves, (b) Ray-path diagrams, (c) WKBJ seismograms computed for the preliminary P-velocity model shown in Fig. 20.

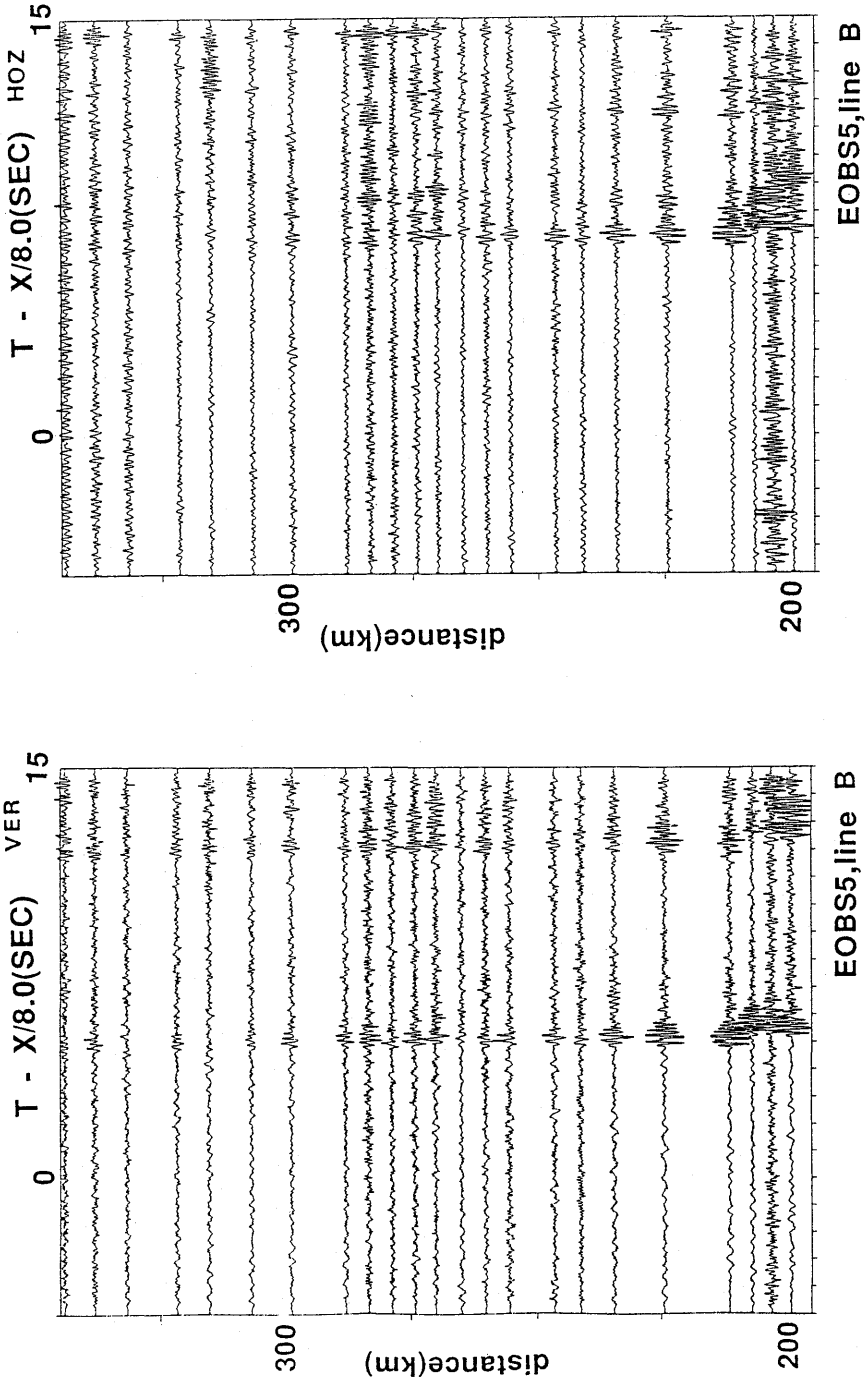

Fig. 22. Record section of EOBS5 for the small explosive shot Line B, (a) vertical component, (b) horizontal component.

In order to test such an interpretation, we performed a model study by ray-tracing, ray-path diagrams, and WKBJ seismograms. An example of a preliminary model calculation which can account for the observed arrival times and wave amplitudes is shown in Fig. 20. Figs. ((a)-(c)) are the calculated travel times, ray paths and seismograms from the model. It is seen that the wide-angle reflections in the distance range of about 350-450 km appear as almost the first arrivals together with P_n. The depth of the reflector is about 20 km beneath the Moho discontinuity. In this calculation, the crustal structure is taken from an average of those reported in section 2. The model shown in Fig. 20, however, does not explain the bending of the phases which are seen at distances closer than 400 km. We suspect that these features are due to some diffraction in the reflection horizon.

Similar phases are seen on the other stations (EOBS5, 4 and 3) for shot line D on the west side of the WNW-ESE direction survey line, but not for the small explosive shots line B on the east side, except at EOBS5, the record of which is shown in Fig. 22 (see Fig. 2). These findings suggest significant heterogeneities in the sub-Moho lithosphere. As stated in section 1, the NNW-SSE survey line is located on the east side of the Nakwe Channel and also along the strike of the fracture zone.

The lateral heterogeneity of the upper mantle may be related to tectonic features. It would be quite natural to think that the fracture zone is related to structures deep inside the upper-mantle, indicating the existence of large scale dynamics.

5. Conclusions

1. In a long range seismic explosion experiment, refractions from sub-Moho high velocity layers were observed in the ENE-WSW direction. This observation does not support the existence of anisotropy in the lithosphere, but indicates a stratified structure in the sub-Moho lithosphere.

2. Wide-angle reflections, possibly from the sub-Moho lithosphere, were recorded at several stations for small explosive shots (20 kg) at a distance range about 350-450 km.

3. Large lateral heterogeneities within the lithosphere were observed, rather than anisotropy.

4. The crust/mantle structure possesses lateral heterogeneity along the survey line in the P-wave velocity profile, which shows a variety of transitions from layer 3 to the mantle.

5. The heterogeneity in the crust/mantle tranisition as well as in the sub-Moho lithosphere may be closely related to the deep sea Nakwe Channel and also to the magnetic fracture zones in this region.

Acknowledgments

We thank the whole shipboard scientific teams, the captain and crew of the survey ships Wakashio-Maru and No. 3 Kaiko-Maru, and supporting staff for their enthusiastic as well as cooperative efforts which have made such a big experiment successful. We thank Dr. Daniel A. Walker, Hawaii Institute of Geophysics, University of Hawaii, for reading the manuscript.

References

ASADA, T. and H. SHIMAMURA, 1976, Observations of earthquakes and explosions at the bottom of the western Pacific: Structure of oceanic lithosphere revealed by long shot experiment, AGU Geophys. Monogr. G.H., SUTTON, M, H. MANGHNANI and R. MOBERLY (eds.), 135-153.

ASADA, T., H. SHIMAMURA, S. ASADA, K. KOBAYASHI and Y. TOMODA, 1984, Explosion seismological experiments on long-range profile in the Northwestern Pacific and the Mariana Sea. AGU Geodynamics series 11, HILDE, T.W.C. and S. UYEDA. (eds.), 105-120.

DUENNEBIER, F.K., B. LIENERT, R. CESSARO, P. ANDERSON and S. MALLICK, 1987, Controlled-source seismic experiment as hole 581C, Init. Repts. DSDP, 88: 105-125, Wash. D.C. (U.S. Govt. Printing Office).

MAMMERICKX, J., 1980, Deep-sea channel in the northwest Pacific, Marine Geology, 34, 207-218.

MAMMERICKX, J. and S.M. SMITH, 1985, Bathymetry of the North-central Pacific, Geological Society of America, Map and Chart series MC-52.

NAGUMO, S., T. OUCHI, J. KASAHARA and S. KORESAWA, 1987, P-wave velocity structure of lithosphere-asthenosphere beneath the Western Northwest Pacific Basin determined by an ocean bottom seismometer array observation, *Bull. Earthq. Res. Inst., University of Tokyo,* 62, 1-18.

SHIMAMURA, H. and T. ASADA, 1984, Velocity anisotropy extending over the entire depth of the oceanic lithosphere. AGU Geodynamics Series 11, HILDE, T.W.C. and UYEDA, S. (eds.), 121-125.

DELP 1986年度　北西太平洋研究航海報告

Part 3　地殻・上部マントルの地震波速度構造

ハワイ大学地球物理研究所　南雲昭三郎

神戸大学理学部地球科学科　久保篤規
大内徹

東京大学地震研究所　片尾浩
是沢定之

1986年度夏に実施された DELP による北西太平洋海域の発破を利用した地震波構造探査によって，この海域の海底地殻下部から上部マントルの地震波速度構造に関して，いくつかの特徴的な解析結果が得られたので報告する．海洋地殻内部及びモホへの漸移形態のみならず，モホ以深に於ける速度構造にも地域的に非一様性がみられる．WSW-ENE 方向の長距離発破測線から得られた記録からは，上部マントルにおける，大規模な速度異方性の存在を支持するような結果は見られなかった．モホ・マントルに関わる地域的非一様性は，海洋地殻第3層に於ける速度の勾配と，モホ面に於ける速度の跳びによって特徴づけられる．モホ以深のリソスフェア内部の何等かの層構造によると思われる広角反射波が，小薬量の発破に依っても 450 km 先まで記録されている．この際だった反射面の存在様式は地震波速度構造の大規模な地域的非一様性と，地磁気によって示されているような破砕帯の存在に深く関係していると考えられる．